Journal of Applied Biology & Biotechnology Vol. 11(5), pp. 112-118, Sep-Oct, 2023
Available online at http://www.jabonline.in
DOI: 10.7324/JABB.2023.138870

# *In vitro* antioxidant and antibacterial potential of biosynthesized yttrium oxide nanoparticles using floral extract of *Illicium verum*

Karthikeyan Kandasamy, Premkumar Kumpati*

Department of Biomedical Science, Bharathidasan University, Trichy, Tamil Nadu, India.

**ARTICLE INFO**

*Article history*:
Received on: April 12, 2023
Accepted on: July 07, 2023
Available online: August 10, 2023

***Key words***:
Yttrium oxide,
*Illicium verum*,
Antibacterial,
Antioxidant,
DPPH.

**ABSTRACT**

Yttrium oxide is one of the rare earth metals. It has an elevated fluorescence emission reliability, which could have applications in biological imaging and photodynamic therapy, particularly in the biomedical field, where it is used as a versatile, multi-dimensional agent with antibacterial, and antioxidant activity. The goal of this research is to synthesize yttrium oxide nanoparticles ($Y_2O_3$ nanoparticles) utilizing [$Y(NO_3)_3$ $6H_2O$] as the precursor and the capping and reducing agent using *Illicium verum* (star anise) extract of flower and the investigation of biomedical applications which are the first report. Green synthesized nanoparticles were characterized with the assistance of a variety of techniques, such as dynamic light scattering, Fourier-transform infrared spectroscopy, X-ray diffraction, and field emission scanning electron microscopy. $Y_2O_3$ nanoparticles exhibited strong antibacterial action against *Staphylococcus aureus* and *Escherichia coli*, with an inhibitory zone measuring 13 mm and 15 mm, respectively. Furthermore, these nanoparticles were able to significantly control bacterial growth in a concentration- and time-dependent manner. *In vitro* antioxidant activity of green-synthesized $Y_2O_3$ nanoparticles was determined using the DPPH technique, and a 50% scavenging efficiency was found at a concentration of 30 µg/mL.

## 1. INTRODUCTION

The distinct morphology of metal oxide nanoparticles is linked to their use in biomedical applications. Due to the differences in particle size between micromaterials and nanomaterials [1], nanoparticle synthesis is a significant obstacle on the road to creating biologically functional materials. As a possible method of transporting drugs, nanoparticles have garnered a lot of interest as cellular imaging labels and vectors for the delivery of genes and growth factors [2-4]. Using nanoparticles in photodynamic and photothermal therapy for tumors are another area of research. Using biosynthesis instead of toxic chemicals has allowed nanoparticle synthesis to advance rapidly in recent years [5].

Recent years have seen intensive study of yttrium oxide ($Y_2O_3$) due to its position as a vital rare earth metal. When it comes to optoelectronics and chemical catalysis, it is one of the most exciting new elements on the horizon. $Y_2O_3$ powder has a high dielectric constant and is very stable at high temperatures [6]. The great efficiency of $Y_2O_3$ as an additive can be put to use in functional composite materials such as yttria-stabilized zirconia films. It is commonly used as a host material for various rare earth dopants, and it is got promising applications in photodynamic therapy and biological imaging [7,8]. Chemical and physical methods of nanoparticle synthesis involve the use of certain toxic substances as reducing and capping agents. However, the biological method of nanoparticle synthesis employed many biological substance and living things [9]. When compared to chemical and physical methods, biosynthesis of nanoparticles resulted in the lower toxicity in highest concentration against non-cancerous cells; thus, biological synthesis has more advantages and is considered a sustainable option [10-12]. Nanoparticles can also be synthesized using biological processes such as those that utilize bacteria, enzymes, and plant extracts, as several authors [13,14] have discussed. The green synthesis of nanoparticles from plant extracts such as bark, leaves, seeds, pods, and tubers has gained popularity in recent years. The hope that this synthesis might benefit human health is a major factor fueling this fascination. Furthermore, recent studies have shown that plant extracts synthesize the greatest amount of nanoparticles when compared to plant powders, which was attributed to the plant powder containing more reducing agents [15]. It is common practice to use plant extracts rich in water-soluble organics and phenolics as reducing agents during the nanoparticle formation process [16,17]. For example, spices and other plant materials rich in phenolic compounds make excellent biomaterials for the creation of nanoparticles. Researchers have found that particular spices make for excellent nanoparticle synthesis platforms.

The synthesis of Yttrium oxide nanoparticles ($Y_2O_3$ nanoparticles) using the star anise (SA) (*Illicium verum*) is discussed in this paper.

*Corresponding Author:
*Premkumar Kumpati,*
*Department of Biomedical Science, Bharathidasan University,*
*Trichy, Tamil Nadu, India.*
*E-mail: prems @ bdu.ac.in*

© 2023 Karthikeyan Kandasamy and Premkumar Kumpati. This is an open access article distributed under the terms of the Creative Commons Attribution License -NonCommercial-ShareAlike Unported License (http://creativecommons.org/licenses/by-nc-sa/3.0/).

Due to its high phenolic content, as reducing agents and capping agent found in SA is reason for better-quality of nanomaterial, and especially polyphenolic components have played a more significant role in inhibiting cancer cell growth in terms of chemical composition than other spices [18]. As a result, the reduction reaction is thought to be extremely fast, resulting in extremely high $Y_2O_3$ nanoparticles productivity and output. This study aims to understand the antibacterial potential against pathogenic bacteria, $Y_2O_3$ nanoparticles have been penetrate the cell wall of microbes and in activate the intracellular proteins and antioxidant potential used diphenyl-1-picrylhydrazile (DPPH) method of green synthesized $Y_2O_3$ nanoparticles using SA is significantly scavenging the free radicals in 1st time reported, which is characterized by field emission scanning electron microscopy (FE-SEM) for used to check the nanoparticles structures after they were synthesized, X-ray diffraction (XRD) for confirms that the synthesized $Y_2O_3$ nanoparticles are a crystalline material, hydrodynamic diameter was measured by dynamic light scattering (DLS), and the occurrence of Y-O-Y and O-Y-O stretching in the synthesized $Y_2O_3$ nanoparticles was further analyzed by Fourier-transform infrared spectroscopy (FTIR).

## 2. MATERIALS AND METHODS

### 2.1. Preparation of Plant Extract

*I. verum* (SA) was purchased from Ghandhi market, Tiruchirappalli district, Tamil Nadu. For this experiment, 20 g of dried SA were mixed with 200 mL of distilled water in a 250 mL Erlenmeyer flask and heated at 60°C for 30 min. Then, the standard filter paper and Whatman No. 1 filter paper were used to refine the crude extract. For research purposes, the filtrate was collected and frozen at 4°C.

### 2.2. Synthesis of Yttrium Oxide Nanoparticles

The Yttrium nitrate hexahydrate [$Y(NO_3)_3$•$6H_2O$] (Sigma Aldrich, USA) has been prepared at a concentration of 0.1M. Then, 10 mL of SA extract was added with 50mL of Yttrium nitrate hexahydrate and stirred at 80°C for 2 h. Following this, the particles were centrifuged for 10 min at 10,000 rpm. Following that, it was washed with deionized water and centrifuged at 1500 rpm for 30 min. After being dried in a hot air oven at 70°C, the sample was mashed in a mortar and pestle. To make $Y_2O_3$ nanoparticles, this powdered material was calcined in a muffle furnace at 500°C [5].

### 2.3. Analytical Characterizations of $Y_2O_3$ Nanoparticles

In FT-IR analysis, SA-mediated $Y_2O_3$ nanoparticles were evaluated using the wavenumber range of 400–4000 $cm^{-1}$ in a Nicolet 6700 spectrophotometer at a rate of 4 $cm^{-1}$ per point. The XRD patterns of nanoparticles were acquired at 45 kV, 40 mA, and a 2 angle 2θ, all of which are typical parameters for recording XRD data (Philips Electronic Instruments Inc., Mahwah, NJ). The hydrodynamic size of $Y_2O_3$ nanoparticles was measured using the DLS analysis method, Zetasizer Nano Instrument. The structural morphology of $Y_2O_3$ nanoparticles was analyzed using FE-SEM. Drying nanoparticles were stored in molds on glass slides. The particles were sputter-coated with gold once they had dried, and JSM-7001F, JEOL, Ltd. of Japan, was used to observe the coating.

### 2.4. Antibacterial Activity Study

#### *2.4.1. Minimum inhibitory concentration (MIC)*

The MIC was determined by the microdilution method using the nutrient broth. The 1 mg/mL of $Y_2O_3$ nanoparticles in the stock solution was dissolved in DMSO, and the various concentrations of the nanoparticles (1, 2.5, 5, 10, 15, 20, 25, 50, 75, and 100 µg/mL from the stock solution were diluted with nutrient broth. 50 µL of each diluted nanoparticle was transferred into wells containing 100 µL of nutrient broth. The total volume was 200 µL, with each well receiving 50 µL of 24-h-old bacterial inoculum. Additions without bacteria are considered a negative control, and the positive control did not add $Y_2O_3$ nanoparticles to the well. The microliter plate was then incubated at 37°C for 24 h. An optical density of turbidity was measured using the Synergy HT Multimode Reader (Biotek, Winooski, USA) at 550 nm. The same experiment was conducted using streptomycin as the standard. All the experiments were performed in triplicates [19,20].

#### *2.4.2. Well diffusion method*

Antibacterial activity by the well-diffusion method of $Y_2O_3$ nanoparticles was examined against *Escherichia coli* and *Staphylococcus aureus*. The plate was pored with Muller–Hinton agar, bacterial suspension was coated uniformly, and then plates were punctured using gel puncture to form wells with a 6 mm diameter. On each well, different concentration of $Y_2O_3$ nanoparticles (25 µg/mL–100 µg/mL) and Streptomycin (HiMedia, India) as positive control (10 µg/mL) and negative control has been used 50 µL autoclaved double distilled water. After that incubating the cultures at 37°C for 24 h, the zone of inhibition (ZOI) was determined by measuring the diameter of the wells (mm) [19].

#### *2.4.3. Turbidimetric method*

Validation of the $Y_2O_3$ nanoparticles' antibacterial efficiency was demonstrated by the turbidimetric technique. Antibacterial activity of $Y_2O_3$ nanoparticles against *E. coli and S. aureus* cultured in Luria Bertani broth. Bacterial cultures that had already been growing for 24 h were inoculated into LB broth that had been spiked with (25 µg/mL to 100 µg/mL of $Y_2O_3$ nanoparticles. As a comparison, LB broth without $Y_2O_3$ nanoparticles was used. After incubating a broth mixture in conical flasks at room temperature with a continuous shaker for 24 h, the optical density was determined at 600 nm to assess the sensitivity of the organisms used in the experiment [5].

### 2.5. Radical Scavenging Activity by the DPPH

The free radical scavenging activity of $Y_2O_3$ nanoparticles was evaluated using the 2, 2-diphenyl-1-picrylhydrazile (DPPH) technique. 100µL of $Y_2O_3$ nanoparticles were prepared at a range of concentrations (10 µg/mL to 50 µg/mL) with ascorbic acid (AA) (Vitamin C) as a positive control. In a 96-well plate, 1 mM DPPH solution was added to each well, and the samples were incubated at room temperature in the dark for 30 min. As measured by a Synergy HT Multimode Reader at 517 nm, the solution's color change from violet to yellow indicated that reactive oxygen species had been scavenged (Biotek, Winooski, USA). The scavenging potential was determined using the following equation:

$$\%\,Inhibition = \frac{Ac - As}{Ac} \times 100$$

Whereas, Ac – OD value of blank, As – OD value of $Y_2O_3$ nanoparticles treated.

## 3. RESULTS AND DISCUSSION

The $Y_2O_3$ nanoparticles were prepared in their pure form using the yttrium nitrate hexahydrate treatment with SA extract solution. The constant stirring carried the precipitate to the settle. The precipitate was

then washed with water and dried in an oven. The powder was finely powdered after drying. FE-SEM, DLS, FTIR, and XRD analyses were used to characterize the grounded sample.

### 3.1. FE-SEM Analysis

The FE-SEM, as shown in [Figure 1], produced pure $Y_2O_3$ nanoparticles using SA extract. The $Y_2O_3$ nanoparticles are spherical in shape and have the additive nature of secondary particles, each of which is composed of a cluster of primary particles and partially agglomerated. The obtained particles had a uniform shape and size, which was confirmed by the FE-SEM. The $Y_2O_3$ nanoparticles exhibit gatherings due to the dipole interaction of every particle. FE-SEM images of yttrium oxide nanoparticles show the formation of a spherical structure, which is found to have a mean approximate size of 150 ± 5 nm.

The hydrodynamic diameter of each particle is determined at a specific position if the nanoparticles are sintered. Similar results were observed in early studies; the nanoparticles were partially aggregated, but the vast majority of them were tightly controlled. Similarly to the previous report [21], the morphological characteristics of the formation of $Y_2O_3$ nanoparticles with spherical shape and 100 nm diameter were analyzed using SEM. The obtained morphological characterization of yttrium oxide nanoparticles was observed to be around 90 nm in particle size with a spherical shape, as likewise reported in early studies [22].

### 3.2. DLS and Zeta Potential Analysis

The DLS analysis revealed the average size of $Y_2O_3$ nanoparticles, which was found to be in the range of 110.4 ± 32 nm. According to the DLS measurements, which show a PDI value of 0.310, the size distribution of the nanoparticles is rather uniform, as shown in [Figure 2]. The production of agglomerated particles in the aqueous medium may be the cause of the increased particle size that was found by DLS, this phenomenon was documented in earlier studies [22]. DLS was primarily used to assess the hydrodynamic size of the $Y_2O_3$ nanoparticles that dissolved in cultured media. These nanoparticles were discovered to be approximately spherical, and throughout the experiment, they showed excellent monodispersity of the synthesized nanoparticles [21].

The surface charge of green synthesized $Y_2O_3$ nanoparticles was analyzed using Zeta potential (ζ), which has a negative charge of −19.2 mV, as shown in [Figure 3], with the capped phenolic compound being responsible for the negative surface charge [23].

### 3.3. FTIR Analysis

Peaks were observed in the FTIR spectrum analyses of $Y_2O_3$ nanoparticles at 3435, 2025,1634,1383,1102, and 676 $cm^{-1}$, as shown in [Figure 4]. The broad spectrum of 3435 $cm^{-1}$ indicates at O-H bend, particles in a solution [24]. The spectrum 2025 $cm^{-1}$ responsible for the strong N=C=S stretching with isothiocyanate functional group. The 1102 cm-1 spectrum is responsible for the strong ether bond with C-O stretching.The sharp peak observed at 1634 $cm^{-1}$ suggested that OH stretching was taking place in the residual moisture [25]. 1383 $cm^{-1}$, which is responsible for the O-H bend, denotes phenol or tertiary alcohol. Y-O stretching in $Y_2O_3$ nanoparticles is responsible for the formation of the bands in the spectrum at around 676 $cm^{-1}$. The peaks in the FTIR spectrum of synthesized $Y_2O_3$ nanoparticles that range between 500 $cm^{-1}$ and 800 $cm^{-1}$ in the previous study can be attributed to the stretching of Y-O molecules that resulted the synthesis of $Y_2O_3$ nanoparticles from the $Y_2O_3$ [11,26].

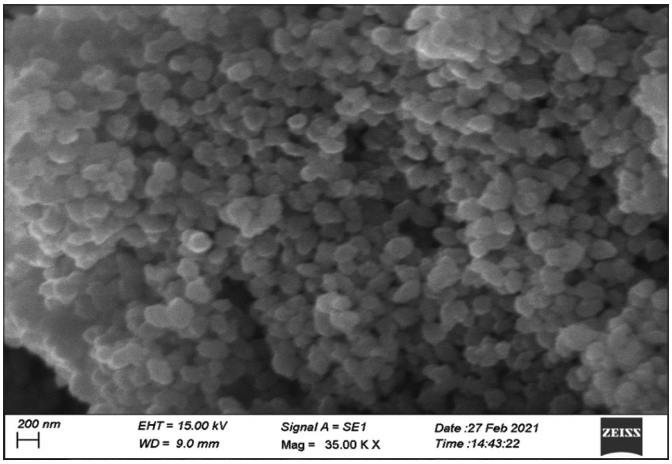


**Figure 1:** FE-SEM image of $Y_2O_3$ nanoparticles.

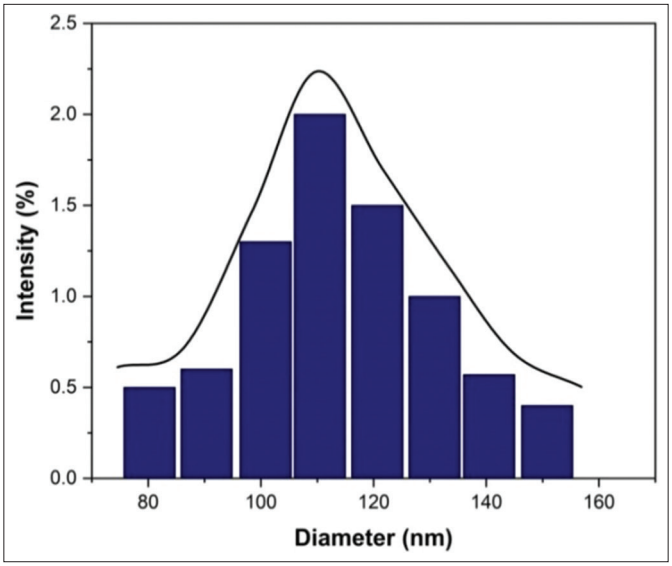


**Figure 2:** DLS analysis of yttrium oxide nanoparticles.

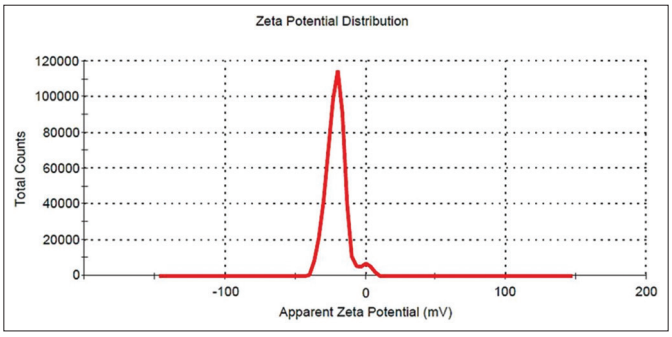


**Figure 3:** Zeta potential analysis of yttrium oxide nanoparticles.

### 3.4. XRD Examination

The XRD patterns of the $Y_2O_3$ nanoparticles, as shown in [Figure 5], depict the crystallized nature of the nanoparticles. This was due to the crystal growth under the lower bath temperature and the accompanied intercalation of nitrate ions from yttrium nitrate. The sample was observed to turn out to be amorphous, and the amorphous nature of the pure sample is shown by a broad hump and the appearance of diffraction peaks. Perhaps

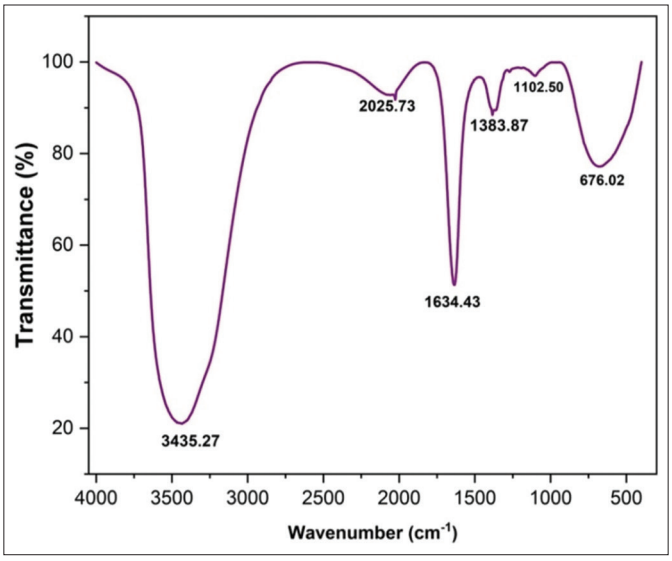


**Figure 4:** FTIR analysis of yttrium oxide nanoparticles.

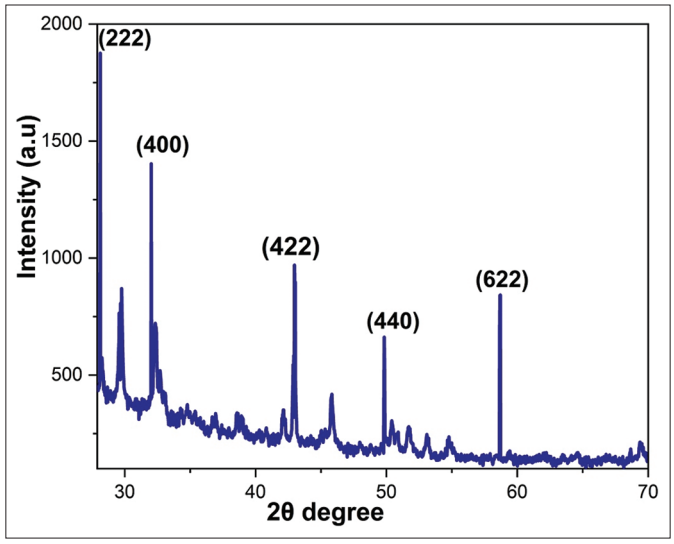


**Figure 5:** XRD of yttrium oxide nanoparticles.

this would indicate that the generated $Y_2O_3$ nanoparticles have the same body-centered cubic shape as the standard $Y_2O_3$ nanoparticles (JCPDF Number 41-1105). The planes of XRD spectra revealed that the prepared $Y_2O_3$ nanoparticles were pure due to the sharp 2θ peaks at 28.1, 33.0°, 43.0°, 49.9°, and 58.8° responsible for the corresponding planes such as 222, 400, 422, 440, and 622. Due to the lingering effects of these other impurities, the XRD data only revealed weak peaks as minor peaks [21].

According to the previous study, 2θ° were observed in 222, 400, 322, 422, 440, and 622 corresponding to the planes with the highest diffraction intensity of biosynthesized $Y_2O_3$ nanoparticles using *Acalypha indica* leaf extract [5], The green synthesized yttrium oxide nanoparticles diffraction peaks appeared at 20.36, 28.91, 33.59, 35.59, 39.54, 43.31, 48.38, 53.11, 57.49, 59.15, 78.32, and 80.95° correspond to the 211, 222, 400, 411, 332, 134, 440, 611, 622, 136, 662, and 048 planes showed crystallographic structure reported in early study [10]. Another report suggested that 2θ° represent that crystallinity of the $Y_2O_3$ nanopowder shown in XRD diffraction peak ranges at 20.54°, 29.18°, 33.71°, 39.84°, 43.49°, 48.62°, and 57.69° which correspond to the planes of 211, 222, 400, 411, 332, 440, and 622 indicate pure $Y_2O_3$ cubic phase [27]. Hence, the present study has been compared with the previous studies that 2θ° peaks were similar in XRD diffraction; the highest diffraction intensity peaks are responsible for the presence of $Y_2O_3$ nanoparticles in crystallite form.

### 3.5. Antibacterial Activity

The antibacterial activity of $Y_2O_3$ nanoparticles has been preliminary investigated using the microdilution method, according to the MIC's OD value, it was evaluated against *E. coli* and *S. aureus* at 10 µg/mL and 15 µg/mL, respectively. The obtained value of MIC was found at the lowest concentration of the nanoparticles, which could not allow any visible pathogenic bacterial growth in the incubation period of 24 h and also after incubation based on OD measurements corresponding to the nanoparticle concentration [19,20].

Research on the efficacy of $Y_2O_3$ nanoparticles as an antibacterial agent was conducted using both Gram-positive (*S. aureus*) and Gram-negative (*E. coli*) harmful bacteria which are generally found in the manmade environment such as soil and water and may cause disease in humans and animals. Since it is the best understood bacterium, *E. coli* serves as a model organism in many antimicrobial susceptibility studies. Diseases

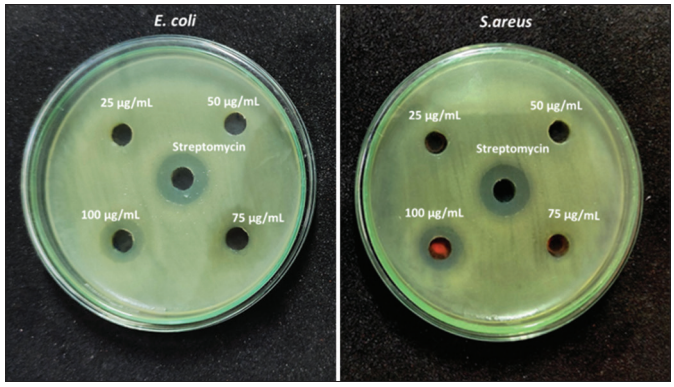


**Figure 6:** Antibacterial activity of $Y_2O_3$ nanoparticles against *Escherichia coli* and *Staphylococcus aureus*.

caused by *S. aureus* range from mild skin infections to potentially fatal endocarditis and toxic shock syndrome. According to [Figure 6], $Y_2O_3$ nanoparticles exhibit a high ZOI high for 100 µg/mL of concentration. This evidence suggests that $Y_2O_3$ nanoparticles generate toxicity for bacteria and cause cell death through interacting with the bacteria's cell membrane. Among the four concentrations, 100 µg/mL had the highest ZOI against *E. coli* (15 mm) and *S. aureus* (13 mm). SA-mediated synthesis $Y_2O_3$ nanoparticles' antibacterial activity may be impacted by their binding to chondrioids and subsequent disruption of the chondrioids' cell division, DNA replication, and respiration processes, all of which contribute directly to cell death. It has been hypothesized that polypenols found in SA kill bacteria directly, activate antibiotics synergistically, and have three distinct ways to reduce bacterial pathogenicity [28]. Moreover, flavonoids have been found to be able to destabilize cytoplasmic membranes, inhibit lactamases and topoisomerase, and hence stop the growth of antibiotic resistance in bacteria [29,30].

Since $Y_2O_3$ nanoparticles bind to the cell membrane by strong electrostatic forces, they are able to effectively suppress the growth of both Gram-positive and Gram-negative bacteria at a concentration of 100 µg/mL. According to the previous reports on the mechanism of antibacterial action of $Y_2O_3$ nanoparticles, yttrium ions may penetrate the cell wall of bacteria and inhibit the growth through down-regulation of enzyme activity, which leads to bacterial cell death [5,31,32].

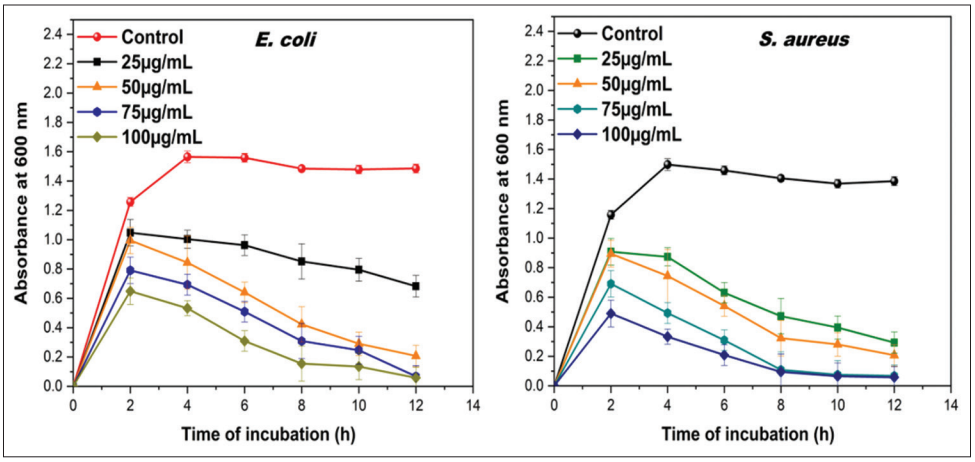


**Figure 7:** Growth curve of *Escherichia coli* and *Staphylococcus aureus* under $Y_2O_3$ nanoparticles treatment.

In contrast to antibiotics, $Y_2O_3$ nanoparticles that were synthesized from the leaf extract of *Lantana camara* (LC) exhibited an excellent inhibitory zone. This was observed in comparison to antibiotics and LC $Y_2O_3$ nanoparticles. The inhibitory zone that was formed by LC $Y_2O_3$ nanoparticles was only marginally larger than the one that was produced by the group that acted as the control. Therefore, LC $Y_2O_3$ nanoparticles are a promising antibacterial for Gram-positive and Gram-negative pathogens such as *Bacillus subtilis* and *E. coli*, as described in a recent report; in addition, $Y_2O_3$ nanoparticles were shown to be active against *E. coli*, *S. marcens*, *P. aerogenosa*, and *S. aureus* [33].

### 3.6. Effect of $Y_2O_3$ Nanoparticles on Bacterial Growth (*E. coli* and *S. aureus*)

Research demonstrating the potential of $Y_2O_3$ nanoparticles on bacterial growth was conducted. [Figure 7] shows the lag, log, stationary, and death phases of the growth curves for *E. coli* and *S. aureus*. The log phase decreased gradually from 25 µg/mL to 100 µg/mL, demonstrating that $Y_2O_3$ nanoparticles had a microbiostatic effect on *E. coli* and *S. aureus* that was dose-dependent. $Y_2O_3$ nanoparticles interact with the treated pathogens, causing cell membrane disruption and a decrease in biomass in a time-dependent way. The use of $Y_2O_3$ nanoparticles has been shown to drastically reduce bacterial growth. UV-visible spectrophotometer readings were used to compare the inhibitory effects of $Y_2O_3$ nanoparticles at various concentrations, 25 µg/mL to 100 µg/mL. Biomass growth was compared before and after the incorporation of $Y_2O_3$ nanoparticles. Increasing the concentration of $Y_2O_3$ nanoparticles inhibits the growth of *E. coli* and *S. aureus*, with the greatest growth inhibition occurring at 100 µg/mL. Similar results were observed in previously reported *A. indica* leaf extract-mediated $Y_2O_3$ nanoparticle synthesis [5].

### 3.7. DPPH Radical Scavenging Activity

The antioxidant activity of $Y_2O_3$ nanoparticles was measured using 2, 2-diphenyl-1-picrylhydrazile (DPPH) and AA as the standard. A freshly produced DPPH solution exhibited a purple color. The purple color changes to yellow when an antioxidant is present in the medium. Thus, antioxidant molecules can eliminate DPPH free radicals and transform them into a colorless or yellow compound, observed at 517 nm absorbance. SA-mediated $Y_2O_3$ nanoparticles showed improved antioxidant properties. An increased concentration of $Y_2O_3$ nanoparticles might be changed from purple to yellow as observed, as shown in Figure 8a. The $IC_{50}$ concentration of scavenging

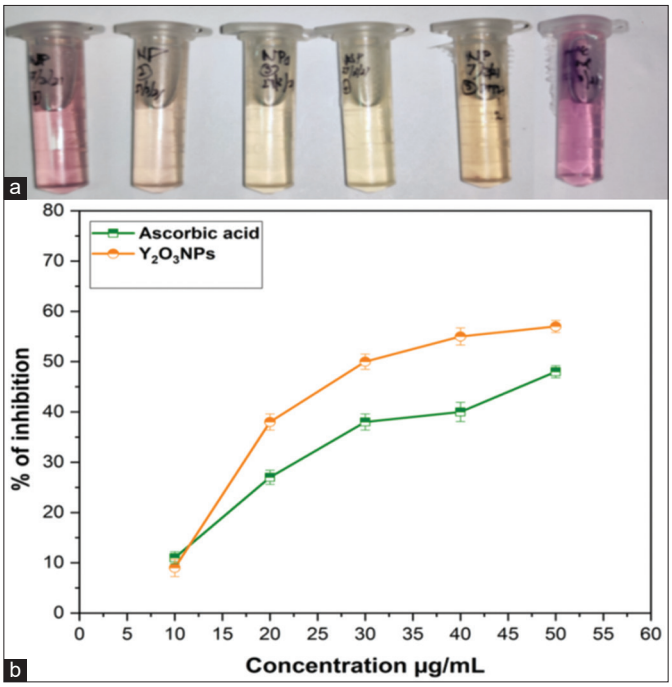


**Figure 8:** Antioxidant activity of $Y_2O_3$ nanoparticles by DPPH method (a) observation of color changes after incubation period and (b) percentage of free radical scavenging activity.

activity, shown in Figure 8b, is 30 µg/mL. This study suggests that this may influence the antioxidant property of $Y_2O_3$ nanoparticles. Similar results were observed and reported as radical scavenging activity for $Y_2O_3$ nanoparticles exposed to significant antioxidant activity as demonstrated by the dose-dependent increase in DPPH radical scavenging activity [22].

The DPPH radical was suppressed at a rate of 22.4% after 5 min, and after an hour, it had reached its highest level, which was 48.1%. According to the findings, Y10 has the capability to reduce DPPH levels, and its antioxidant activity grows with time, reaching its maximum level an hour after treatment has been delivered. In addition, the antioxidant activity of yttrium oxide nanocrystallites increases as time dependent. The improvement of antioxidant activity is strongly dependent on the particle size, as was established in the past with several other kinds of materials, such as iron oxide nanoparticles [34].

This behavior has previously been observed in materials that are relatively comparable in terms of the composition of their make-up. It is quite likely that this effect is a consequence of the increased surface area that may be accomplished by carrying out the suggested synthesis with the use of P-123 from previous research [35]. It has been demonstrated that poly EGMP, also known as ethylene glycol methacrylate phosphate-functionalized core-shell $Y_2O_3$ nanoparticles, has direct antioxidant effects *in vivo*, where they are able to block or eliminate the ROS that is necessary to destroy the cells. As a consequence of this, $Y_2O_3$ has been demonstrated to be neuroprotective as well as an efficient antioxidant, in particular in the presence of programmed cell death and oxidative stress. Therefore, it is acceptable to draw the conclusion that $Y_2O_3$ nanoparticles can assist neuronal cell survival in the face of oxidative stress, which may have implications for therapeutic use as reported [36,37].

## 4. CONCLUSION

In the progression of this research, $Y_2O_3$ nanoparticles were created by synthesizing an extract of SA blossoms, which have a high level of surface reactivity as well as biocompatibility. A number of different spices have been identified by researchers as having excellent qualities for the synthesis of nanoparticles. A substance that is high in phenolic compounds is necessary for the formation of nanoparticles, and SA is the only spice that delivers sufficient quantities of these components. The characterization of the spherical form of $Y_2O_3$ nanoparticles was accomplished through the use of FE-SEM. To identify the properties of the nanoparticle, different types of techniques were utilized. There is not a publication that has been found that describes the free radical scavenging and antibacterial activity of $Y_2O_3$ nanoparticles that have been synthesized using a flower extract of SA. It has been demonstrated that some chemical components of SA, such as the phenolic compounds that it contains, can prevent the growth of bacteria, including *S. aureus* and *E. coli.* The findings indicate that green-synthesized $Y_2O_3$ nanoparticles can be employed well in biological applications.

## 5. ACKNOWLEDGMENTS

The authors express their gratitude to Bharathidasan University for having received Department of Science and Technology Science and Engineering Research Board Empowerment and Equity (DST-SERB-EEQ), Government of India, project fellow Ref. No. 03056/P4/2019 Dated June 28, 2019.

## 6. AUTHORS' CONTRIBUTIONS

Karthikeyan Kandhasamy: Investigation, methodology, writing-original draft, editing, and review. Kumpati Premkumar: Project administration, validation conceptualization, supervision, writing-review, and editing.

## 7. CONFLICTS OF INTEREST

The authors declare that they have no conflicts of interest.

## 8. ETHICAL APPROVALS

This study does not involve experiments on animal or human subjects.

## 9. DATA AVAILABILITY

The data that are supporting the findings of the study are available within the article.

## 10. PUBLISHER'S NOTE

This journal remains neutral with regard to jurisdictional claims in published institutional affiliation.

## REFERENCES

1. Wu L, Jimmy CY, Zhang L, Wang X, Li S. Selective self-propagating combustion synthesis of hexagonal and orthorhombic nanocrystalline yttrium iron oxide. J Solid State Chem 2004;177:3666-74.
2. Soppimath KS, Aminabhavi TM, Kulkarni AR, Rudzinski WE. Biodegradable polymeric nanoparticles as drug delivery devices. J Control Release 2001;70:1-20.
3. Hood JD, Bednarski M, Frausto R, Guccione S, Reisfeld RA, Xiang R, ***et al***. Tumor regression by targeted gene delivery to the neovasculature. Science 2002;296:2404-7.
4. Chung YI, Tae G, Hong Yuk S. A facile method to prepare heparin-functionalized nanoparticles for controlled release of growth factors. Biomaterials 2006;27:2621-6.
5. Kannan SK, Sundrarajan M. Biosynthesis of Yttrium oxide nanoparticles using *Acalypha indica* leaf extract. Bull Mater Sci 2015;38:945-50.
6. Hirai T, Kawamura Y, Komasawa I. Preparation of Y2O3 nanoparticulate thin films using an emulsion liquid membrane system. J Colloid Interface Sci 2004;275:508-13.
7. Chang M, Tie S. Fabrication of novel luminor Y(2)O(3):Eu(3+)@ SiO(2)@YVO(4): Eu(3+) with core/shell heteronanostructure. Nanotechnology 2008;19:075711.
8. Andelman T, Gordonov S, Busto G, Moghe PV, Riman RE. Synthesis and cytotoxicity of $Y_2O_3$ nanoparticles of various morphologies. Nanoscale Res Lett 2009;5:263-73.
9. Mohanpuria P, Rana NK, Yadav SK. Biosynthesis of nanoparticles: Technological concepts and future applications. J Nanopart Res 2008;10:507-17.
10. Nagajyothi PC, Pandurangan M, Veerappan M, Kim DH, Sreekanth TV, Shim J. Green synthesis, characterization and anticancer activity of yttrium oxide nanoparticles. Mater Lett 2018;216:58-62.
11. Augustine R, Dalvi YB, Yadu Nath VK, Varghese R, Raghuveeran V, Hasan A, *et al*. Yttrium oxide nanoparticle loaded scaffolds with enhanced cell adhesion and vascularization for tissue engineering applications. Mater Sci Eng C Mater Biol Appl 2019;103:109801.
12. Selvaraj V, Bodapati S, Murray E, Rice KM, Winston N, Shokuhfar T, ***et al***. Cytotoxicity and genotoxicity caused by yttrium oxide nanoparticles in HEK293 cells. Int J Nanomedicine 2014;9:1379-91.
13. Shankar SS, Rai A, Ahmad A, Sastry M. Rapid synthesis of Au, Ag, and bimetallic Au core-Ag shell nanoparticles using Neem (*Azadirachta indica*) leaf broth. J Colloid Interface Sci 2004;275: 496-502.
14. Narayanan KB, Sakthivel N. Coriander leaf mediated biosynthesis of gold nanoparticles. Mater Lett 2008;62:4588-90.
15. Sathishkumar M, Sneha K, Won SW, Cho CW, Kim S, Yun YS. *Cinnamom zeylanicum* bark extract and powder mediated green synthesis of nano-crystalline silver particles and its bactericidal activity. Colloids Surf B Biointerfaces 2009;73:332-8.
16. Huang J, Li Q, Sun D, Lu Y, Su Y, Yang X, *et al*. Biosynthesis of silver and gold nanoparticles by novel sundried *Cinnamomum camphora* leaf. Nanotechnology 2007;18:105104.
17. Sathishkumar M, Sneha K, Kwak IS, Mao J, Tripathy SJ, Yun YS. Phyto-crystallization of palladium through reduction process using *Cinnamom zeylanicum* bark extract. J Hazard Mater 2009;171:400-4.
18. Shan B, Cai YZ, Sun M, Corke H. Antioxidant capacity of 26 spice extracts and characterization of their phenolic constituents. J Agric Food Chem 2005;53:7749-59.
19. Pop OL, Mesaros A, Vodnar DC, Suharoschi R, Tăbăran F, Mageruşan L, ***et al***. Cerium oxide nanoparticles and their efficient

antibacterial application *in vitro* against gram-positive and gram-negative pathogens. Nanomaterials (Basel) 2020;10:1614.
20. Gnanam S, Ashokkumar R, SenthilKannan K. Antimicrobial activity of the novel metal oxide nanoparticles against selected human pathogenic bacteria. IOP Conf Ser Mater Sci Eng 2019;561:012086.
21. Zhou G, Li Y, Ma Y, Liu Z, Cao L, Wang D, *et al*. Size-dependent cytotoxicity of yttrium oxide nanoparticles on primary osteoblasts *in vitro*. J Nanopart Res 2016;18:1-4.
22. Khurana A, Anchi P, Allawadhi P, Kumar V, Sayed N, Packirisamy G, ***et al***. Yttrium oxide nanoparticles reduce the severity of acute pancreatitis caused by cerulein hyperstimulation. Nanomedicine 2019;18:54-65.
23. Esmaeilzadeh Kenari R, Razavi R. Phenolic profile and antioxidant activity of free/bound phenolic compounds of sesame and properties of encapsulated nanoparticles in different wall materials. Food Sci Nutr 2022;10:525-35.
24. Srinivasan R, Yogamalar R, Bose AC. Structural and optical studies of yttrium oxide nanoparticles synthesized by co-precipitation method. Mater Res Bull 2010;45:1165-70.
25. Wang H, Zhu JJ, Zhu JM, Liao XH, Xu S, Ding T, *et al*. Preparation of nanocrystalline ceria particles by sonochemical and microwave assisted heating methods. Phys Chem Chem Phys 2002;4:3794-9.
26. Mitra RN, Merwin MJ, Han Z, Conley SM, Al-Ubaidi MR, Naash MI. Yttrium oxide nanoparticles prevent photoreceptor death in a light-damage model of retinal degeneration. Free Radic Biol Med 2014;75:140-8.
27. Benammar I, Salhi R, Deschanvres JL, Maalej R. The effect of rare earth element (Er, Yb) doping and heat treatment on suspension stability of Y2O3 nanoparticles elaborated by sol-gel method. J Mater Res Technol 2020;9:12634-42.
28. Cushnie TP, Lamb AJ. Recent advances in understanding the antibacterial properties of flavonoids. Int J Antimicrob Agents 2011;38:99-107.
29. Daglia M. Polyphenols as antimicrobial agents. Curr Opin Biotechnol 2012;23:174-81.
30. Xie Y, Chen J, Xiao A, Liu L. Antibacterial activity of polyphenols: Structure-activity relationship and influence of hyperglycemic condition. Molecules 2017;22:1913.
31. Bassous NJ, Garcia CB, Webster TJ. A study of the chemistries, growth mechanisms, and antibacterial properties of cerium- and yttrium-containing nanoparticles. ACS Biomater Sci Eng 2021;7:1787-807.
32. Magdalane CM, Kaviyarasu K, Vijaya JJ, Siddhardha B, Jeyaraj B. Facile synthesis of heterostructured cerium oxide/yttrium oxide nanocomposite in UV light induced photocatalytic degradation and catalytic reduction: Synergistic effect of antimicrobial studies. J Photochem Photobiol B 2017;173:23-34.
33. Govindasamy R, Govindarasu M, Alharthi SS, Mani P, Bernaurdshaw N, Gomathi T, ***et al***. Sustainable green synthesis of yttrium oxide ($Y_2O_3$) nanoparticles using *Lantana camara* leaf extracts: Physicochemical characterization, photocatalytic degradation, antibacterial, and anticancer potency. Nanomaterials (Basel) 2022;12:2393.
34. Das D, Nath BC, Phukon P, Kalita A, Dolui SK. Synthesis of ZnO nanoparticles and evaluation of antioxidant and cytotoxic activity. Colloids Surf B Biointerfaces 2013;111:556-60.
35. Mellado-Vázquez R, García-Hernández M, López-Marure A, López-Camacho PY, de Jesús Morales-Ramírez Á, Beltrán-Conde HI. Sol-gel synthesis and antioxidant properties of yttrium oxide nanocrystallites incorporating P-123. Materials (Basel) 2014;7:6768-78.
36. Schubert D, Dargusch R, Raitano J, Chan SW. Cerium and yttrium oxide nanoparticles are neuroprotective. Biochem Biophys Res Commun 2006;342:86-91.
37. Kassem S, Arafa MM, Yehya MM, Soliman MA. *In vivo* study of dose-dependent antioxidant efficacy of functionalized core-shell yttrium oxide nanoparticles. Naunyn Schmiedebergs Arch Pharmacol 2022;395:593-606.

**How to cite this article:**
Kandasamy K, Kumpati P. *In vitro* antioxidant and antibacterial potential of biosynthesized yttrium oxide nanoparticles using floral extract of *Illicium verum*. J App Biol Biotech. 2023;11(5):112-118.
DOI:10.7324/JABB.2023.138870